

Raman spectroscopy as probe of nanometer-scale strain variations in graphene

C. Neumann^{1,2}, S. Reichardt¹, P. Venezuela³, M. Drögeler¹, L. Banszerus¹, M. Schmitz¹, K. Watanabe⁴, T. Taniguchi⁴, F. Mauri⁵, B. Beschoten¹, S. V. Rotkin^{1,6}, and C. Stampfer^{1,2}

¹ JARA-FIT and 2nd Institute of Physics, RWTH Aachen University, 52074 Aachen, Germany

² Peter Grünberg Institute (PGI-9), Forschungszentrum Jülich, 52425 Jülich, Germany

³ Instituto de Física, Universidade Federal Fluminense, 24210-346 Niterói, RJ, Brazil

⁴ National Institute for Materials Science, 1-1 Namiki, Tsukuba, 305-0044, Japan

⁵ IMPMC, UMR CNRS 7590, Sorbonne Universités UPMC Univ. Paris 06,

MNHN, IRD, 4 Place Jussieu, 75005 Paris, France

⁶ Department of Physics and Center for Advanced Materials and Nanotechnology, Lehigh University, Bethlehem, Pennsylvania 18015, USA

(Dated: October 30, 2021)

Confocal Raman spectroscopy is a versatile, non-invasive investigation tool and a major workhorse for graphene characterization. Here we show that the experimentally observed Raman 2D line width is a measure of nanometer-scale strain variations in graphene. By investigating the relation between the G and 2D line at high magnetic fields we find that the 2D line width contains valuable information on nanometer-scale flatness and lattice deformations of graphene, making it a good quantity for classifying the structural quality of graphene even at zero magnetic field.

Graphene combines several highly interesting material properties in a unique way, promising unprecedented material functionalities. This makes graphene increasingly attractive for industrial applications¹ but, at the same time, stresses the need for non-invasive characterization techniques. In recent years, Raman spectroscopy has proven to be highly useful as a non-invasive method not only to identify graphene^{2,3}, but also to extract information on local doping⁴⁻⁷, strain^{8,9} and lattice temperature^{10,11}. Even more insights can be gained when utilizing confocal, scanning Raman spectroscopy to study spatially resolved doping domains^{7,12}, edge effects^{3,13} and position dependent mechanical lattice deformations, including strain¹⁴⁻¹⁶. The spatial resolution of so-called Raman maps is on the order of the laser spot size (which for confocal systems is typically on the order of 500 nm) and the extracted quantities (such as doping or strain) are in general averaged over the spot size. It is therefore important to distinguish between length scales significantly larger or smaller than the laser spot size. In particular, we will distinguish between strain variations on a *micrometer scale*, which can be extracted from spatially resolved Raman maps, and *nanometer-scale* strain variations, which are on sub-spot-size length scales and cannot be directly observed by Raman imaging, but are considered as important sources of scattering for electronic transport¹⁷.

Here we show that the experimentally observed Raman 2D line width is a measure of nanometer-scale strain variations in graphene on insulating substrates, i.e. it contains valuable information on local (i.e. nanometer-scale) flatness, lattice deformations and crystal quality of graphene. To prove that the the experimentally observed 2D line width depends on sub-spot size strain variations and lattice deformations we employ the following strategy:

(i) We start by showing that by combining Raman spectroscopy with magnetic fields, electronic broadening

contributions for the Raman G line width can be strongly suppressed. Since in perpendicular magnetic fields the electronic states in graphene condense into Landau levels (LLs), the interaction between electronic excitations and lattice vibrations becomes B field dependent. In agreement with existing theory¹⁸⁻²¹ and experiments^{22,23}, we demonstrate that by applying a perpendicular B field of around 8 T, the G line does as good as not depend on electronic properties such as charge carrier doping, screening or electronic broadening.

(ii) We observe that, under these conditions, the G line width nevertheless exhibits strong variations across graphene flakes. In particular, we show that the G line width is significantly increased in regions where the graphene flake features bubbles and folds, i.e. in correspondence with increased structural deformations.

(iii) Finally, we show that at 8 T there is a (nearly) linear dependence between the G line width and the 2D line width, implying that there is a common source of line broadening. According to points (i) and (ii) the broadening must be related to structural lattice deformations. This finding is further supported by a detailed analysis of the relation between the area of the 2D peak and its line width. By analyzing the relation between the G and 2D line width, we find that nm-scale strain variations constitute a dominant contribution to the observed line broadenings. Importantly, the 2D line has been shown to be only very weakly dependent on the B field²⁴, meaning that no magnetic field is required to extract information on nm-scale strain variations from the 2D line width, which makes this quantity interesting for practical applications.

For the low temperature Raman measurements, we employ a commercially available confocal Raman setup that allows us to perform spatially-resolved experiments at a temperature of 4.2 K and magnetic fields of up to 9 T. We use an excitation laser wavelength of 532 nm with a spot diameter on the sample of around 500 nm. For detection,

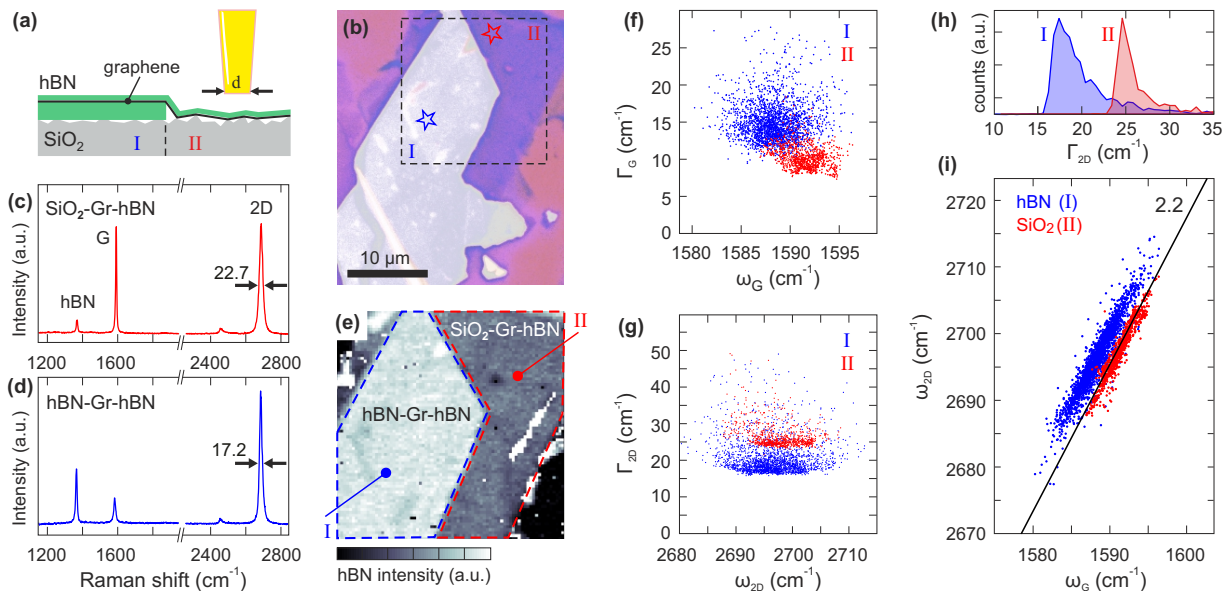


FIG. 1. (color online) (a) Schematic cross section of the investigated sample highlighting the different regions I and II. (b) Optical image of a Gr-hBN heterostructure resting partly on hBN and SiO₂. (c) and (d) Raman spectrum taken on the SiO₂-Gr-hBN (c) and hBN-Gr-hBN (d) areas. The positions where the spectra were taken are marked by a blue and a red star, respectively, in panel (b). (e) Raman map of the intensity of the hBN peak. The dashed lines mark the regions I and II. (f) Γ_G versus ω_G recorded on various spots on regions I (blue) and II (red) of the sample. (g) Γ_{2D} versus ω_{2D} recorded on various spots on regions I (blue) and II (red) of the sample. (h) Histograms of Γ_{2D} recorded on various spots on regions I (blue) and II (red) of the sample. (i) ω_{2D} versus ω_G recorded on various spots on regions I (blue) and II (red) of the sample.

we use a single mode optical fiber and a CCD spectrometer with a grating of 1200 lines/mm. All measurements are performed with linear laser polarization and a $\times 100$ objective.

The investigated graphene (Gr) sheet is partly encapsulated in hexagonal boron nitride (hBN) and partly sandwiched between SiO₂ and hBN as illustrated in Figure 1a. An optical image of our sample is shown in Figure 1b. In contrast to graphene encapsulated in hBN, graphene flakes supported by SiO₂ usually feature lower carrier mobilities of around 10^3 - 10^4 cm²/(Vs), indicating a detrimental influence of SiO₂ on the electronic properties of graphene. In this regard, our structure gives us the invaluable capability of probing a single graphene sheet exposed to two different substrates (region I and II in Figures 1a and 1b). The sample is fabricated with a dry and resist-free transfer process following refs. 25 and 26, where we pick up an exfoliated graphene flake with an hBN flake and deposit it onto the hBN-SiO₂ transition area of the substrate. A typical Raman spectrum of graphene supported by SiO₂ and covered by hBN, taken at the position of the red star in Figure 1b, is shown in Figure 1c. The characteristic hBN line as well as the graphene G and 2D lines can be clearly identified. At first glance, the spectra recorded in the hBN-Gr-hBN area look similar (see Figure 1d, taken at the position marked by the blue star in Figure 1b). However, it is evident that the ratio between the 2D and G line intensity is higher in this case. Furthermore, the full width at half

maximum (FWHM) of the 2D line, Γ_{2D} , is significantly smaller.

The confocal nature of our Raman setup enables us to do spatially resolved measurements. An example of a Raman map is shown in Figure 1e, where the spatially resolved intensity of the hBN line is depicted. The hBN and SiO₂ areas can be clearly distinguished in the map (see highlighted regions I and II). When analyzing the Raman spectra of every point on the map, one finds that the G lines recorded in the hBN-encapsulated area are broader than in the SiO₂ supported area (compare red and blue data points in Figure 1f). This is a clear indication of reduced charge carrier doping induced by the hBN substrate compared to SiO₂. In fact, at low charge carrier doping, the phonon mode can decay into electron-hole pairs, which results in a broadening of the G peak^{5,27}. For the 2D line, in contrast, the Γ_{2D} recorded in the hBN-encapsulated area is mostly between 16 cm⁻¹ and 20 cm⁻¹, while it is above 22 cm⁻¹ in the SiO₂ area (see blue and red curves in the histogram of Figure 1h, respectively). Note that both Γ_{2D} and Γ_G do not show a dependence on the respective frequencies ω_{2D} and ω_G (Figures 1f and 1g). In Figure 1i the position of the G and 2D lines for every spectrum obtained on the investigated graphene sheet are displayed. For both substrates, the data points scatter along a line with a slope of 2.2. This slope coincides with the ratio of strain induced shifts (i.e. of the related Grüneisen parameters) of the Raman G and 2D modes²⁸. This indicates that there are sig-

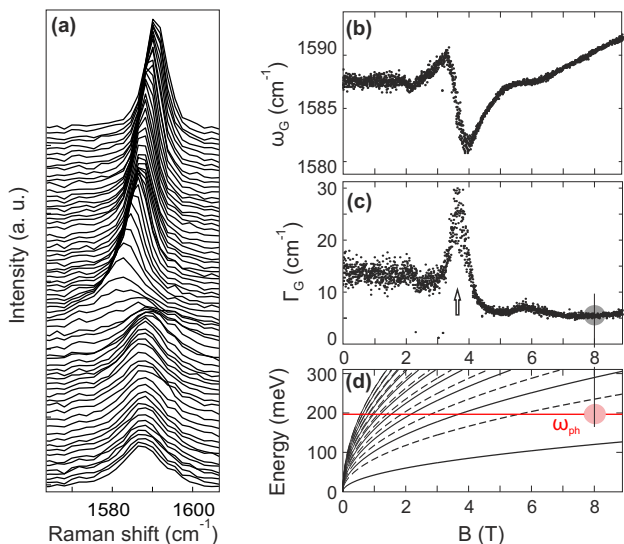


FIG. 2. (color online) (a) Raman spectra recorded as a function of magnetic field, ranging from 0 T (bottom spectrum) to 8.9 T (top spectrum). The spectra are vertically offset for clarity. (b) and (c) Frequency, ω_G , and FWHM, Γ_G , of the G peak as a function of magnetic field as obtained from Lorentzian fits to the data shown in panel (a). The arrow in panel (c) showcases a value of the magnetic field at which the phonon is energetically matched to a LL transition. (d) Evolution of the energies of LL transitions with magnetic field. The full lines represent inter-band transitions in which the LL index changes by one. The dashed lines represent inter-band transitions in which the LL index does not change. The red line represents the G mode phonon frequency at zero B field. The circled region in (c) and (d) highlights the region in which no LL transitions energetically match the G mode phonon.

nificant strain variations on both substrates across the entire graphene layer. Assuming the strain to be of biaxial nature, the spread of the data points translates into a maximum, micrometer-scale strain variation of about 0.14%²⁸. The offset of the SiO₂ and hBN data points can be understood in terms of the higher charge carrier doping induced by the SiO₂ substrate, which shifts the data points toward higher values of ω_G ⁵, and differences in the dielectric screening of hBN and SiO₂ that effectively shift the 2D line position²⁹. Since the data stems from a single graphene flake that has undergone identical fabrication steps for both substrate regions, the difference in charge carrier doping is unambiguously due to the two different substrate materials.

For a more refined comparison of the Raman spectra on both substrates, we seek to suppress the effects on the G line, arising from these differences in charge carrier doping. We therefore minimize the influence of the electronic system on the Raman G line by applying a perpendicular magnetic field. In the presence of a perpendicular magnetic field, the electronic states in graphene condense into Landau levels (LLs). The coupling of these Landau levels to the G mode is well understood^{18,19} and experimentally confirmed^{21–23,30–35}. When a LL transition energetically

matches the G mode phonon, the position of the G line is shifted and its line width increases. An example for the evolution of the Raman G peak with magnetic field, taken on the hBN sandwich area, is shown in Figure 2a. The individual spectra are offset for clarity. For a detailed analysis, single Lorentzians are fitted to every spectrum. The resulting frequency, ω_G , and FWHM, Γ_G , are displayed in Figures 2b and 2c, respectively. The arrow at $B = 3.7$ T (Figure 2c) indicates a value of the magnetic field where a LL transition is energetically matched with the phonon, leading to a broadening of the G line. However, at a magnetic field of about 8 T, no LL transition is close to the G mode, as illustrated in Figure 2d, where the energies of the relevant LL transitions as a function of magnetic field are compared to the energy of the G mode phonon. Consequently at this high magnetic field the influence of the electronic system on the position and width of the G line is minimized. Note that this effect is independent of the charge carrier density and the exact values of the broadening of the LL transitions assuming that the latter are within a reasonable range as found by other studies^{23,34}. Thus, the residual broadening of the G line is most likely determined by phonon-phonon scattering and averaging effects over different strain values that vary on a nanometer scale (i.e. sub-spot size length scale see also Supplementary Information).

To show that this applies to the entire sample, we first show that the broadening of the electronic states is low enough on the entire hBN-Gr-hBN area. In Figures 3a and 3b, we show maps of Γ_G at $B = 0$ T and 3.8 T, respectively. On the hBN part, the width of the G line shows the resonant behavior depicted in Figure 2c (see also histogram in Figure 3d). This effect happens on all spots on the hBN area, independent of the local doping and strain values and independent of possible local folds and bubbles. The suppression of magneto-phonon resonances on the SiO₂ substrate can be attributed to the higher charge carrier density. At higher charge carrier density the needed LL transitions are blocked by the Pauli principle. In a next step, we tune the magnetic field to 8 T, where the electronic influences on the Raman G line are at a minimum. A map of Γ_G over the entire flake at a magnetic field of 8 T is shown in Figure 3c. Distinct features across the whole sample are visible as regions with increased line width. A comparison with a scanning force microscope image of the sample (Figure 3e) reveals that many of these regions can be associated with folds and bubbles most likely induced during the fabrication process, some of which even cross the border between the underlying hBN and SiO₂ substrate regions.

As electronic broadening effects are suppressed at 8 T, the increased line width of the G line in the vicinity of these lattice deformations arises from enhanced phonon-phonon scattering and/or an averaging effect over varying nm-scale strain conditions.

Interestingly, the same features can also be identified in a Γ_{2D} map recorded at $B = 0$ T, shown in Figure 3f. This

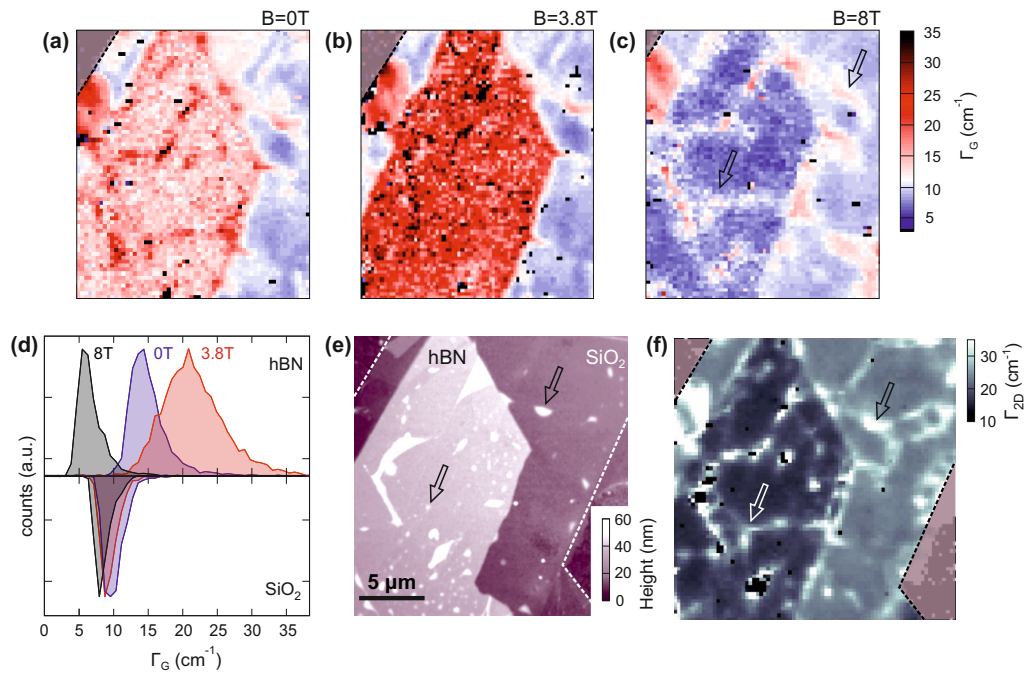


FIG. 3. (color online) (a), (b), and (c) Raman maps of the FWHM of the G peak, Γ_G , taken at different magnetic fields, i.e. $B = 0$ T (a), 3.8 T (b), and 8 T (c), respectively. The different regions I and II (labeled in Figure 1a) can be well distinguished in all three panels. (d) Histograms of Γ_G for the different magnetic fields, $B = 0$ T (blue), 3.8 T (red), $B = 8$ T (gray) and the two substrate substrates hBN (top panel) and SiO₂ (bottom panel). (e) Scanning force microscope (SFM) image of the investigated sample. (f) Raman map of Γ_{2D} recorded at 0 T. The arrows highlight mechanical folds visible in the SFM image as well as in the Raman maps (see panels (c), (e), and (f)).

strongly suggests that the lattice deformations identified at 8 T in Γ_G also cause a broadening of the 2D mode. The same trend is highlighted in Fig. 4a, where we show the relation of Γ_G and Γ_{2D} for all recorded Raman spectra at 8 T. The additional teal data points stem from a graphene-on-SiO₂ sample and the orange star originates from a different hBN-Gr-hBN sandwich structure with all data having been obtained at 8 T. Notably, the points from all substrate regions lie on one common line. From this linear relation between Γ_{2D} and Γ_G (Figure 4a), we conclude that there must be a common source of line broadening, which is connected to structural deformations. This is mainly due to the fact that at 8 T the G-line broadening is only very weakly affected by electronic contributions (see above). The range of the presented scatter plot can be extended by including data recorded on low-quality graphene samples with significant doping, as shown in Figure 4b. Here, no magnetic field but high doping (corresponding to Fermi energies much higher than half of the phonon energy $\hbar\omega_{\text{ph}}/2 \approx 100$ meV) is used to suppress Landau damping of the G mode, leaving Γ_G unaffected from electronic contributions. The colored data points are from Raman maps ($B = 0$ T) of CVD (chemical vapor deposition)-grown graphene flakes that were transferred onto SiO₂ by a wet chemistry-based transfer. These graphene sheets contain doping values of $n_{\text{el}} > 3 \times 10^{12} \text{ cm}^{-2}$, which corresponds to Fermi energies, $E_F > 200$ meV (see suppl. material). The data

points show the same trend as the values obtained at 8 T (gray data points in Figure 4b) and even extend the total range of the dependence to higher values of Γ_{2D} .

While the linear relation between Γ_G and Γ_{2D} in Figure 4a and 4b shows that structural deformations also broaden the 2D line, it is less straightforward to identify the actual mechanism of broadening. It is, in principle, possible that the high values of Γ_{2D} around folds and bubbles are due to a combination of increased phonon-phonon scattering, averaging effects over different strain values within the laser spot and reduced electronic life times. However, interestingly the slopes in Figures 4a and 4b are around 2.2 (see black lines). This is a remarkable resemblance to the strain induced frequency shifts of both modes (compare Figure 1i). This provides very strong indication that averaging over different strain values, which vary on a nanometer scale (see Fig. 4c), play an important role in the broadening of the experimentally observed 2D line. This averaging effect broadens the G and 2D line by the same ratio as their peak positions shift for fixed average strain values explaining the slope of 2.2 between Γ_G and Γ_{2D} (see Supplementary Information). We are aware that the low charge carrier densities in the hBN encapsulated area might result in a narrowing of the 2D mode by three to four wave numbers³⁶. However, the large differences of Γ_{2D} on the order of 20-30 cm⁻¹ on both substrates cannot be explained by the differences in charge carrier doping^{7,36,37}.

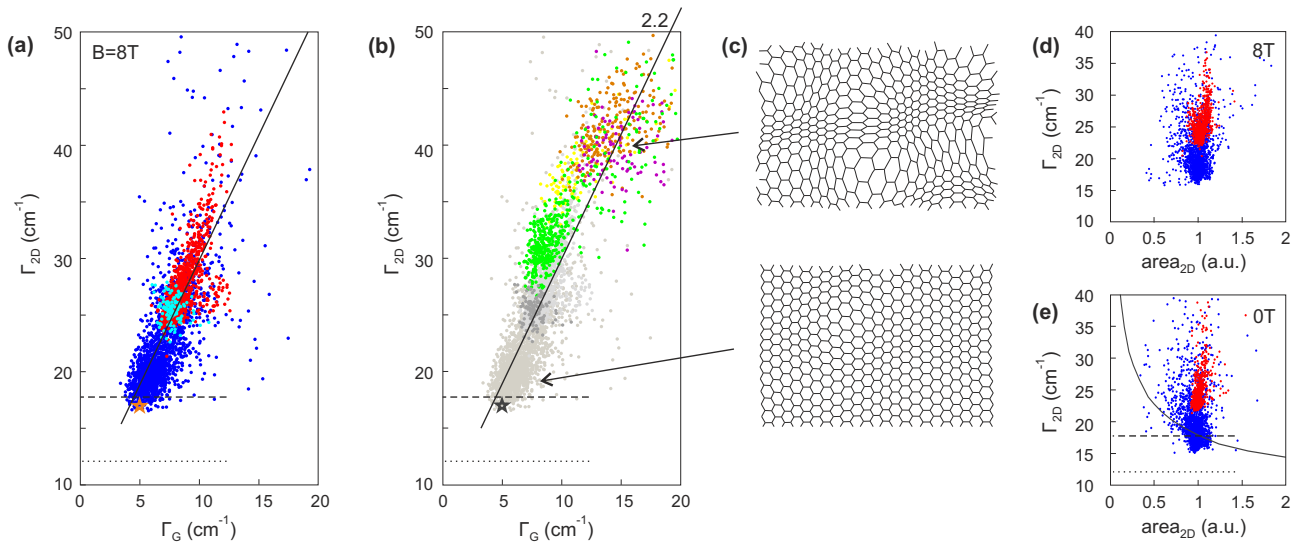


FIG. 4. (color online) (a) Γ_G versus Γ_{2D} recorded on various points on the hBN part (blue) and SiO₂ (red) of the sample at a magnetic field of 8 T. Additional data points from a graphene-on-SiO₂ sample (teal) and a second hBN-Gr-hBN sample (orange star) are shown. (b) The data points of panel (a) are depicted in gray. The colored data are recorded on four different CVD graphene flakes on SiO₂ substrate at 0 T. All four samples have doping values of $n_{el} > 3 \times 10^{12}$, such that Landau damping of the G line is suppressed. The dashed and dotted lines in panels (a) and (b) indicate the calculated values of Γ_{2D} from DFT calculations including electron-phonon and phonon-phonon broadening (dotted line) and electron-phonon, electron-electron and phonon-phonon broadening (dashed line). (c) Two schematic illustrations of nanometer-scale strain variations (top: large variations, bottom: small variations). (d) Γ_{2D} versus the integrated area of the 2D peak as obtained from single Lorentzian fits for the hBN part (blue) and SiO₂ (red) measured at 8 T. Both data clouds are scaled to an average $area_{2D}$ value of one. (e) Similar plot as in panel (d) but for 0 T. The solid black line is the calculated dependence of Γ_{2D} and $area_{2D}$ for varying electronic broadening from the DFT calculations, specified in the text and in ref. 37. The dashed and dotted black lines are the same as in panel (a) and (b).

Interestingly, the lowest Γ_{2D} observed in our experiments are very close to the value that we compute from first-principles as in ref. 37 (see Supplementary Information for details) assuming an undoped, defect-free and stress-free sample of graphene (horizontal dashed and dotted lines in Figures 4a and 4b). In such an approach, the width of the 2D peak is determined by the anharmonic decay rate of the two phonons involved (5.3 cm⁻¹ according to ref. 38), and, indirectly, by the broadening of the electron and hole, denoted as γ in ref. 37, (see also ref. 39). According to ref. 37, the electron-phonon contribution to γ is 81.9 meV for electronic states in resonance with the 2.33 eV laser-light. With such a value of γ we obtain a Γ_{2D} of 12.1 cm⁻¹ (dotted lines in Figures 4a, 4b and 4e). If, following ref. 40, we double such value of γ to account for the electron-electron scattering, we obtain a Γ_{2D} of 17.9 cm⁻¹ (dashed lines in Figures 4a, 4b and 4e), in close agreement with the lowest measured values. In principle, the observed increase of Γ_{2D} with respect to its minimum value could be attributed to an increase of the electronic broadening γ , due to doping (increasing the electron-electron scattering) or to the presence of defects (increasing the electron-defect scattering)^{37,39,41}. By investigating the relation between Γ_{2D} and the integrated area of the 2D peak ($area_{2D}$) we can exclude such a hypothesis. In Figures 4d and 4e we show scatter plots of Γ_{2D} versus the region-normalized $area_{2D}$ for

both $B = 8$ T and 0 T, highlighting the very weak B-field dependence of Γ_{2D} . More importantly, we observe that the area of the 2D peak does not depend on Γ_{2D} , contrary to what is expected in presence of a variation of the electronic broadening γ ^{37,39,41}. In particular the measured data does not follow the calculated dependence of Γ_{2D} on $area_{2D}$, reported in Fig. 4e, obtained in the calculation by varying electronic broadening γ . This dismisses differences in the electronic broadening as a main mechanism for the observed variations of Γ_{2D} .

Finally, our finding that the 2D line depends on nanometer-scale strain inhomogeneities is also in good agreement with high resolution scanning tunneling microscopy measurements, which reveal that graphene on SiO₂ forms short-ranged corrugations, while graphene on hBN features significantly more flat areas⁴².

In summary, we showed that by using a magnetic field of 8 T to strongly suppress the influence of the electronic contributions on the Raman G line width, the latter can be used as a measure for the amount of nm-scale strain variations. Most importantly, we observed a nearly linear dependence between the G and 2D line widths at 8 T independent of the substrate material, indicating that the dominating source of the spread of the broadening of both peaks is the same. From the slope $\Delta\Gamma_{2D}/\Delta\Gamma_G$ of around 2.2, we deduce that averaging effects over nanometer-scale strain variations make a major contribution to this

trend. Since the 2D line width shows only a very weak dependence on the B field, this quantity can even be used without a magnetic field to gain information on the local strain homogeneity and thus on the structural quality of graphene. These insights can be potentially very valuable for monitoring graphene fabrication and growth processes in research and industrial applications, where a fast and non-invasive control of graphene lattice deformations is

of great interest.

ACKNOWLEDGMENT

We thank T. Khodkov for support during the measurements. Support by the Helmholtz Nanoelectronic Facility (HNF), the DFG, the ERC (GA-Nr. 280140) and the EU project Graphene Flagship (contract no. NECT-ICT-604391), are gratefully acknowledged. P.V. acknowledges financial support from the Capes-Cofecub agreement.

-
- ¹ K. S. Novoselov, V. Fal'ko, L. Colombo, P. Gellert, M. Schwab, and K. Kim, *Nature* **490**, 192 (2012).
 - ² A. Ferrari, J. Meyer, V. Scardaci, C. Casiraghi, M. Lazzeri, F. Mauri, S. Piscanec, D. Jiang, K. Novoselov, S. Roth, and A. Geim, *Phys. Rev. Lett.* **97**, 187401 (2006).
 - ³ D. Graf, F. Molitor, K. Ensslin, C. Stampfer, A. Jungen, C. Hierold, and L. Wirtz, *Nano Lett.* **7**, 238 (2007).
 - ⁴ A. C. Ferrari, *Solid State Commun.* **143**, 47 (2007).
 - ⁵ J. Yan, Y. Zhang, P. Kim, and A. Pinczuk, *Phys. Rev. Lett.* **98**, 166802 (2007).
 - ⁶ S. Pisana, M. Lazzeri, C. Casiraghi, K. S. Novoselov, A. K. Geim, A. C. Ferrari, and F. Mauri, *Nat. Mater.* **6**, 198 (2007).
 - ⁷ C. Stampfer, F. Molitor, D. Graf, K. Ensslin, A. Jungen, C. Hierold, and L. Wirtz, *Appl. Phys. Lett.* **91**, 241907 (2007).
 - ⁸ M. Mohr, J. Maultzsch, and C. Thomsen, *Phys. Rev. B* **82**, 201409 (2010).
 - ⁹ M. Huang, H. Yan, T. F. Heinz, and J. Hone, *Nano Lett.* **10**, 4074 (2010).
 - ¹⁰ I. Calizo, A. Balandin, W. Bao, F. Miao, and C. Lau, *Nano Lett.* **7**, 2645 (2007).
 - ¹¹ A. A. Balandin, S. Ghosh, W. Bao, I. Calizo, D. Teweldebrhan, F. Miao, and C. N. Lau, *Nano Lett.* **8**, 902 (2008).
 - ¹² M. Drögeler, F. Volmer, M. Wolter, B. Terrés, K. Watanabe, T. Taniguchi, C. Guntherodt, C. Stampfer, and B. Beschoten, *Nano Lett.* **14**, 6050 (2014).
 - ¹³ C. Casiraghi, A. Hartschuh, H. Qian, S. Piscanec, C. Georgi, A. Fasoli, K. Novoselov, D. Basko, and A. Ferrari, *Nano Letters* **9**, 1433 (2009).
 - ¹⁴ T. Mohiuddin, A. Lombardo, R. Nair, A. Bonetti, G. Savini, R. Jalil, N. Bonini, D. Basko, C. Galiotis, N. Marzari, *et al.*, *Phys. Rev. B* **79**, 205433 (2009).
 - ¹⁵ J. Zabel, R. R. Nair, A. Ott, T. Georgiou, A. K. Geim, K. S. Novoselov, and C. Casiraghi, *Nano Lett.* **12**, 617 (2012).
 - ¹⁶ D. Yoon, Y.-W. Son, and H. Cheong, *Phys. Rev. Lett.* **106**, 155502 (2011).
 - ¹⁷ N. J. Couto, D. Costanzo, S. Engels, D.-K. Ki, K. Watanabe, T. Taniguchi, C. Stampfer, F. Guinea, and A. F. Morpurgo, *Phys. Rev. X* **4**, 041019 (2014).
 - ¹⁸ T. Ando, *J. Phys. Soc. Jpn.* **76**, 024712 (2007).
 - ¹⁹ M. Goerbig, J.-N. Fuchs, K. Kechedzhi, and V. I. Fal'ko, *Phys. Rev. Lett.* **99**, 087402 (2007).
 - ²⁰ O. Kashuba and V. I. Fal'ko, *New J. Phys.* **14**, 105016 (2012).
 - ²¹ C. Qiu, X. Shen, B. Cao, C. Cong, R. Saito, J. Yu, M. S. Dresselhaus, and T. Yu, *Phys. Rev. B* **88**, 165407 (2013).
 - ²² J. Yan, S. Goler, T. D. Rhone, M. Han, R. He, P. Kim, V. Pellegrini, and A. Pinczuk, *Phys. Rev. Lett.* **105**, 227401 (2010).
 - ²³ C. Neumann, S. Reichardt, M. Drögeler, B. Terrés, K. Watanabe, T. Taniguchi, B. Beschoten, S. V. Rotkin, and C. Stampfer, *Nano Lett.* **15**, 1547 (2015).
 - ²⁴ C. Faugeras, P. Kossacki, D. Basko, M. Amado, M. Sprinkle, C. Berger, W. A. de Heer, and M. Potemski, *Phys. Rev. B* **81**, 155436 (2010).
 - ²⁵ L. Wang, I. Meric, P. Huang, Q. Gao, Y. Gao, H. Tran, T. Taniguchi, K. Watanabe, L. Campos, D. Muller, J. Guo, P. Kim, J. Hone, K. Shepard, and C. Dean, *Science* **342**, 614 (2013).
 - ²⁶ S. Engels, B. Terrés, F. Klein, S. Reichardt, M. Goldsche, S. Kuhlen, K. Watanabe, T. Taniguchi, and C. Stampfer, *physica status solidi (b)* **251**, 2545 (2014).
 - ²⁷ C. Casiraghi, S. Pisana, K. Novoselov, A. Geim, and A. Ferrari, *Appl. Phys. Lett.* **91**, 233108 (2007).
 - ²⁸ J. E. Lee, G. Ahn, J. Shim, Y. S. Lee, and S. Ryu, *Nat. Commun.* **3**, 1024 (2012).
 - ²⁹ F. Forster, A. Molina-Sanchez, S. Engels, A. Epping, K. Watanabe, T. Taniguchi, L. Wirtz, and C. Stampfer, *Phys. Rev. B* **88**, 085419 (2013).
 - ³⁰ C. Faugeras, M. Amado, P. Kossacki, M. Orlita, M. Kühne, A. A. Nicolet, Y. I. Latyshev, and M. Potemski, *Phys. Rev. Lett.* **107**, 036807 (2011).
 - ³¹ C. Faugeras, P. Kossacki, A. Nicolet, M. Orlita, M. Potemski, A. Mahmood, and D. Basko, *New J. Phys.* **14**, 095007 (2012).
 - ³² C. Faugeras, M. Amado, P. Kossacki, M. Orlita, M. Sprinkle, C. Berger, W. A. De Heer, and M. Potemski, *Phys. Rev. Lett.* **103**, 186803 (2009).
 - ³³ P. Kossacki, C. Faugeras, M. Kühne, M. Orlita, A. Mahmood, E. Dujardin, R. Nair, A. Geim, and M. Potemski, *Phys. Rev. B* **86**, 205431 (2012).
 - ³⁴ Y. Kim, J. Poumirol, A. Lombardo, N. Kalugin, T. Georgiou, Y. Kim, K. Novoselov, A. Ferrari, J. Kono, O. Kashuba, V. Fal'ko, and D. Smirnov, *Phys. Rev. Lett.* **110**, 227402 (2013).
 - ³⁵ P. Leszczynski, Z. Han, A. A. Nicolet, B. A. Piot, P. Kossacki, M. Orlita, V. Bouchiat, D. M. Basko, M. Potemski, and C. Faugeras, *Nano Lett.* **14**, 1460 (2014).
 - ³⁶ S. Berciaud, X. Li, H. Htoon, L. E. Brus, S. K. Doorn, and T. F. Heinz, *Nano Lett.* **13**, 3517 (2013).

- ³⁷ P. Venezuela, M. Lazzeri, and F. Mauri, *Phys. Rev. B* **84**, 035433 (2011).
- ³⁸ L. Paulatto, F. Mauri, and M. Lazzeri, *Phys. Rev. B* **87**, 214303 (2013).
- ³⁹ D. M. Basko, *Phys. Rev. B* **78**, 125418 (2008).
- ⁴⁰ F. Herzig, M. Calandra, P. Gava, P. May, M. Lazzeri, F. Mauri, and J. Maultzsch, *Phys. Rev. Lett.* **113**, 187401 (2014).
- ⁴¹ D. M. Basko, S. Piscanec, and A. Ferrari, *Phys. Rev. B* **80**, 165413 (2009).
- ⁴² C.-P. Lu, G. Li, K. Watanabe, T. Taniguchi, and E. Y. Andrei, *Phys. Rev. Lett.* **113**, 156804 (2014).